BULLETIN DE L'ASSOCIATION MINERALOGIQUE DU CANADA

THE CANADIAN MINERALOGIST

JOURNAL OF THE MINERALOGICAL ASSOCIATION OF CANADA

Volume 32 September 1994 Part 3

The Canadian Mineralogist
Vol. 32. pp. 477-489 (1994)

STRUCTURAL ASPECTS OF OXIDATION–DEHYDROGENATION IN STAUROLITE

FRANCA CAUCIA, ATHOS CALLEGARI, ROBERTA OBERTI, LUCIANO UNGARETTI AND FRANK C. HAWTHORNE*

CNR - Centro di Studio per la Cristallochimica e la Cristallografia, via Bassi 4, I-27100 Pavia, Italy

ABSTRACT

The oxidation–dehydrogenation mechanism in natural staurolite has been investigated by single-crystal structure refinement of crystals heated in air at a series of temperatures up to 950°C. Crystal structures were refined in the space group *C2/m* to *R* indices of 1–2% using graphite-monochromated Mo*K*α X-radiation. With increasing temperature of annealing, the site populations changed dramatically. The degree of Al–□ order over the *M*(3*A*) and *M*(3*B*) sites decreases with increasing temperature; this is accompanied by a reduction in the β angle, the latter being a measure of the spontaneous strain. Thus with increasing temperature, the degree of order in the structure decreases, and the structure approaches orthorhombic symmetry. However, a new cation site, *T*(3), becomes important in the heated structure, appearing with very low occupancy in the structure annealed at 500°C; with increasing temperature of annealing, the occupancy of the site increases dramatically (to 1.10 apfu) as the occupancies of the other sites decrease, particularly *M*(3*A*), *M*(3*B*) and *T*(2). The *T*(3) site is occupied by Al and Fe^{3+}, and is tetrahedrally coordinated by the O(1*A*), O(1*B*) and 2 × O(3) oxygen atoms. The oxidation–dehydrogenation proceeds *via* oxidation of Fe^{2+} at *T*(2), with the loss of an associated hydrogen atom at one of the coordinating O(1*A*) or O(1*B*) hydroxyl anions; this oxidation is accompanied by major rearrangement of cations that involves all cation sites except *T*(1). The presence of cations at the *T*(3) site in natural staurolite is hence an indicator of postcrystallization oxidation–dehydrogenation.

Keywords: staurolite, oxidation, dehydrogenation, crystal-structure refinement.

SOMMAIRE

Nous avons étudié le mécanisme d'oxydation – déshydrogénation dans la staurotide naturelle par affinement de la structure de cristaux chauffés dans l'air à des paliers atteignant 950°C. Les affinements ont été effectués dans le groupe spatial *C2/m* jusqu'à un résidu *R* entre 1 et 2% en utilisant un rayonnement Mo*K*α avec monochromatisation au graphite. A mesure qu'augmente la température, la population des sites change de façon dramatique. Le degré d'ordre impliquant Al et □ sur les sites *M*(3*A*) et *M*(3*B*) diminue avec l'augmentation de la température, et l'angle β, mesure de la déformation spontanée, diminue aussi. C'est donc dire qu'avec une augmentation de la température, le degré d'ordre dans la structure diminue, et celle-ci se rapproche d'une symétrie orthorhombique. Toutefois, un nouveau site cationique, *T*(3), devient important dans la structure chauffée. Ce site possède un taux d'occupation très faible dans la structure équilibrée à 500°C; à une température plus élevée, le taux d'occupation augmente de façon remarquable, jusqu'à 1.10 atomes par unité formulaire, à mesure que le taux

* Escaped temporarily from the Department of Geological Sciences, University of Manitoba, Winnipeg, Manitoba R3T 2N2.

d'occupation des autres sites diminue, en particulier $M(3A)$, $M(3B)$ et $T(2)$. Ce sont Al et Fe^{3+} qui occupent le site $T(3)$, qui est en coordinence avec O(1*A*), O(1*B*) et 2 × O(3) (atomes d'oxygène). Le processus d'oxydation – déshydrogénation procède par oxydation de Fe^{2+} dans le site $T(2)$, avec la perte d'un atome d'hydrogène associé à un groupe hydroxyle du site O(1*A*) ou O(1*B*). Cette étape est accompagnée d'une ré-organisation importante des cations de tous les sites sauf $T(1)$. La présence de cations sur le site $T(3)$ dans la staurotide naturelle serait donc une indication d'oxydation – déshydrogénation suite à la cristallisation.

(Traduit par la Rédaction)

Mots-clés: staurotide, oxydation, déshydrogénation, affinement de la structure cristalline.

INTRODUCTION

Staurolite is a complex rock-forming silicate mineral that has been the focus of a considerable amount of attention in the last few years. The results of detailed chemical (Dutrow *et al.* 1986, Holdaway *et al.* 1986a, b), structural (Ståhl *et al.* 1988, Alexander 1989, Hawthorne *et al.* 1993a, b, c) and spectroscopic (Dyar *et al.* 1991, Henderson *et al.* 1993) work have finally led to a more satisfactory picture of its crystal chemistry. This is of particular interest as staurolite is an important indicator mineral in metamorphic rocks, and thermodynamic measurements, thermodynamic modeling and field observations usually lead to mutually contradictory conclusions (*e.g.*, Pigage & Greenwood 1982, Holdaway *et al.* 1988).

Hawthorne *et al.* (1993c) wrote the chemical formula of staurolite as $A_4B_4C_{16}D_4T_8O_{40}X_8$, where A = □, Fe^{2+} and Mg (□ ≥ 2), B = Fe^{2+}, Zn, Co, Mg, Al, Li, Mn^{2+} and □, C = Al, Mg and (Fe^{3+}, Cr, V, Ti), D = Al, □ and Mg? (□ ≥ 2), T = Si and Al, and X = OH, F and O. Holdaway *et al.* (1986a, b) noted that in some cases (specifically their samples EH–6 and M–1), staurolite probably contains significantly higher Fe^{3+} than other samples, and Dyar *et al.* (1991) resolved a significant doublet in the Mössbauer spectrum of staurolite EH–6 that could be assigned to Fe^{3+} in tetrahedral coordination. Hawthorne *et al.* (1993a) identified an additional tetrahedrally coordinated site [designated $T(3)$] of very low occupancy in some crystals of staurolite; on the basis of local stereochemistry, they tentatively assigned minor Fe^{3+} to this site. The stereochemistry of $T(3)$ suggests that the occupancy of this site results from a locally coupled oxidation–dehydrogenation process. In order to verify this mechanism of reaction, we have followed the changes in staurolite after heating in air at a series of increasing temperatures. We note that most temperatures of heating used here are above the maximum temperature-stability of staurolite, but the crystal metastably persists above its stability limit. When we use the term "equilibrium", we are referring to the oxidation and cation-ordering reactions, and do not intend to infer that staurolite is the equilibrium phase at the conditions of heating. The results of these heating experiments are presented here.

EXPERIMENTAL

The staurolite used in this work was found in sands from the Ticino River, Italy; its chemical composition is given in Table 1, together with the cell content calculated on the basis of 46.5 O [= $O_{45}(OH)_3$]. This specific crystal was selected for two reasons: (i) there is a close correspondence between the Fe^{2+} and OH contents, and hence, in principle, both oxidation *and* dehydrogenation could proceed to completion; (ii) the β angle differs significantly from 90°, and hence the progress of convergent ordering as a function of temperature also can be followed. EMP (Electron MicroProbe) data and room-temperature crystal-structure refinement were reported in Hawthorne *et al.* [1993a, crystal S(36)]. Here we compare those data with those obtained from X-ray structure refinement at room temperature after annealing the crystal at 500, 600, 700, 800, 900 and 950°C. To be sure that equilibrium was reached, we heated the crystal for 5 h at 500°C, and then for another 5 h at 500°C, collecting intensity data after each heating. After 5 h heating, there were significant changes in the structure, particularly with regard to the refined site-scattering values. The further 5 h heating produced no additional changes in the structure, indicating that the crystal had come to equilibrium within 5 hours at 500°C. Thus the 24 h heating time at the higher temperatures was more than sufficient to ensure equilibrium. The sequence of heating experiments was repeated for another crystal

TABLE 1. CHEMICAL COMPOSITION AND UNIT FORMULA* FOR THE STAUROLITE OF THIS WORK

SiO_2	27.32	Si	7.576
Al_2O_3	55.49	Al	0.424
TiO_2	0.55		8.000
Cr_2O_3	0.04	Al	17.713
Fe_2O_3[+]	0.45	Ti	0.115
FeO	12.98	Fe^{3+}	0.094
MgO	1.60	Fe^{2+}	3.010
MnO	0.16	Mg	0.661
CoO	0.03	Mn	0.038
ZnO	0.21	Zn	0.043
	98.83	**	29.674

* calculated on the basis of 46.5 Ox
** includes 0.009 Cr and 0.007 Co
[+] see Dyar *et al.* (1991)

of (slightly) different composition, but the results for that crystal were not materially different from the results for crystal S(36); consequently, only the latter are reported here.

X-ray data collection

The crystal was attached to a glass fiber and mounted on a Philips PW 1100 automated four-circle diffractometer and examined with graphite-monochromated Mo$K\alpha$ X-radiation. Unit-cell dimensions were calculated by least-squares refinement of the setting angles of 48 aligned reflections throughout the range $-35 < \theta < 35°$; results are given in Table 2. Intensity data were collected for all hkl and $h\bar{k}l$ reflections over the range $2 < \theta < 45°$ (40° for the 500°C data), except for the 500°C data, for which the weak reflections were not collected; data were reduced as described by Hawthorne *et al.* (1993a). After the data collection, the crystal was detached from the glass fiber, heated in a furnace and then quenched; X-ray intensity data were then re-collected. This process was repeated at different (higher) temperatures on the same crystal; Table 2 shows the conditions of annealing, the

TABLE 2. CELL DIMENSIONS* AND MISCELLANEOUS INFORMATION CONCERNING DATA COLLECTION AND STRUCTURE REFINEMENT OF HEATED STAUROLITE

Temp. (°C)	25	500	600	700	800	900	950
Time (hours)	–	10	24	24	24	24	24
a (Å)	7.864	7.866	7.865	7.867	7.861	7.860	7.860
b	16.619	16.621	16.612	16.619	16.638	16.645	16.645
c	5.659	5.658	5.648	5.625	5.604	5.606	5.606
β (°)	90.17	90.15	90.04	90.00	90.00	90.00	90.00
V (Å^3)	739.5	739.7	737.9	735.4	732.8	733.5	733.5
# of $\|F\|$	2272	1249	1516	1871	1756	1753	2074
# of $\|F\|_{obs}$	2112	1249	1318	1690	1539	1525	1860
R_{sym}	1.9	–	1.4	1.2	1.0	1.5	1.0
R_{all}	2.2	1.9	2.2	1.7	1.6	1.7	1.6
R_{obs}	1.9	1.9	1.6	1.3	1.1	1.2	1.2

* $\sigma < 1$ in last figure

TABLE 3. ATOMIC POSITIONS* AND EQUIVALENT ISOTROPIC DISPLACEMENT FACTORS (Å) FOR HEATED STAUROLITE

T (°C)		23°C	500°C (5h)	500°C (5+5)h	600°C	700°C	800°C	900°C	950°C
O(1A)	x	0.23340	0.23396	0.23391	0.23536	0.23706	0.23846	0.23849	0.23863
	y	0	0	0	0	0	0	0	0
	z	0.96302	0.96357	0.96353	0.96507	0.96789	0.97078	0.97081	0.97069
	B_{eq}	0.67	0.68	0.67	0.74	0.84	0.85	0.89	0.84
O(1B)	x	0.23618	0.23602	0.23608	0.23581	0.23697	0.23845	0.23862	0.23863
	y	0	0	0	0	0	0	0	0
	z	0.53372	0.53370	0.53377	0.53402	0.53201	0.52943	0.52906	0.52918
	B_{eq}	0.72	0.73	0.75	0.77	0.84	0.84	0.87	0.84
O(2A)	x	0.25552	0.25536	0.25544	0.25517	0.25556	0.25579	0.25573	0.25582
	y	0.16153	0.16157	0.16161	0.16153	0.16179	0.16199	0.16200	0.16199
	z	0.01537	0.01501	0.01526	0.01533	0.01475	0.01422	0.01427	0.01430
	B_{eq}	0.41	0.43	0.43	0.44	0.46	0.48	0.48	0.44
O(2B)	x	0.25437	0.25440	0.25444	0.25482	0.25553	0.25582	0.25572	0.25591
	y	0.16126	0.16130	0.16136	0.16153	0.16181	0.16198	0.16198	0.16204
	z	0.48387	0.48344	0.48402	0.48456	0.48524	0.48579	0.48573	0.48559
	B_{eq}	0.43	0.46	0.45	0.44	0.46	0.48	0.48	0.44
O(3)	x	0.00177	0.00187	0.00146	0.00196	0.00258	0.00355	0.00353	0.00352
	y	0.08894	0.08916	0.08897	0.08917	0.09003	0.09087	0.09094	0.09093
	z	0.24523	0.24666	0.24630	0.24895	0.25000	0.25010	0.24983	0.24994
	B_{eq}	0.63	0.66	0.65	0.64	0.69	0.70	0.71	0.67
O(4)	x	0.02154	0.02169	0.02161	0.02150	0.02143	0.02109	0.02112	0.02114
	y	0.24918	0.24925	0.24933	0.24930	0.24994	0.25054	0.25059	0.25056
	z	0.24963	0.24970	0.24954	0.24974	0.25002	0.25005	0.25013	0.24988
	B_{eq}	0.42	0.42	0.43	0.43	0.45	0.46	0.46	0.42
O(5)	x	0.52700	0.52714	0.52706	0.52677	0.52524	0.52420	0.52428	0.52433
	y	0.10039	0.10031	0.10021	0.09984	0.09861	0.09770	0.09755	0.09780
	z	0.24952	0.24964	0.24957	0.24991	0.24996	0.25000	0.25002	0.24995
	B_{eq}	0.40	0.41	0.42	0.43	0.47	0.51	0.52	0.47
T(1)	x	0.13413	0.13412	0.13412	0.13432	0.13470	0.13490	0.13490	0.13489
	y	0.16602	0.16610	0.16611	0.16631	0.16720	0.16813	0.16817	0.16811
	z	0.24851	0.24881	0.24884	0.24962	0.25002	0.25002	0.24998	0.25000
	B_{eq}	0.29	0.31	0.31	0.32	0.38	0.41	0.42	0.37
T(2)	x	0.39198	0.39153	0.39154	0.38949	0.38248	0.38002	0.38022	0.38015
	y	0	0	0	0	0	0	0	0
	z	0.24777	0.24839	0.24821	0.24965	0.25001	0.25001	0.25007	0.25002
	B_{eq}	1.17	1.15	1.16	1.15	0.83	0.53	0.59	0.56

TABLE 3. continued

T (°C)		23°C	500°C (5h)	500°C (5+5)h	600°C	700°C	800°C	900°C	950°C
T(3)	*x*	0.12500	0.13363	0.13932	0.12856	0.12508	0.12597	0.12589	0.12589
	y	0	0	0	0	0	0	0	0
	z	0.25000	0.25193	0.24292	0.25020	0.24989	0.25006	0.25012	0.25010
	B_{eq}	0.36	0.39	0.42	0.39	0.44	0.47	0.50	0.46
M(1A)	*x*	1/2	1/2	1/2	1/2	1/2	1/2	1/2	1/2
	y	0.17527	0.17520	0.17508	0.17480	0.17407	0.17342	0.17339	0.17345
	z	0	0	0	0	0	0	0	0
	B_{eq}	0.36	0.35	0.40	0.39	0.40	0.42	0.42	0.38
M(1B)	*x*	1/2	1/2	1/2	1/2	1/2	1/2	1/2	1/2
	y	0.17510	0.17507	0.17510	0.17481	0.17407	0.17340	0.17338	0.17345
	z	1/2	1/2	1/2	1/2	1/2	1/2	1/2	1/2
	B_{eq}	0.36	0.39	0.42	0.39	0.41	0.42	0.42	0.42
M(2)	*x*	0.26336	0.26338	0.26336	0.26355	0.26365	0.26418	0.26421	0.26424
	y	0.41087	0.41702	0.41071	0.41100	0.41202	0.41266	0.41261	0.41259
	z	0.25170	0.25133	0.25142	0.25035	0.25000	0.24997	0.24999	0.24997
	B_{eq}	0.47	0.49	0.51	0.53	0.54	0.57	0.57	0.53
M(3A)	*x*	0	0	0	0	0	0	0	0
	y	0	0	0	0	0	0	0	0
	z	0	0	0	0	0	0	0	0
	B_{eq}	0.43	0.50	0.45	0.45	0.48	0.46	0.48	0.41
M(3B)	*x*	0	0	0	0	0	0	0	0
	y	0	0	0	0	0	0	0	0
	z	1/2	1/2	1/2	1/2	1/2	1/2	1/2	1/2
	B_{eq}	0.42	0.43	0.43	0.44	0.49	0.48	0.48	0.42
M(4A)	*x*	1/2	1/2	1/2	1/2	1/2	1/2	1/2	1/2
	y	0	0	0	0	0	0	0	0
	z	0	0	0	0	0	0	0	0
	B_{eq}	0.75	0.85	0.85	1.00	0.85	0.86	0.88	0.95
M(4B)	*x*	1/2	1/2	1/2	1/2	1/2	1/2	1/2	1/2
	y	0	0	0	0	0	0	0	0
	z	1/2	1/2	1/2	1/2	1/2	1/2	1/2	1/2
	B_{eq}	0.80	0.88	1.01	1.04	0.86	0.89	0.91	0.90

* standard deviations are <5 in the last decimal place

cell dimensions after each treatment, and details of the data collection and reduction.

Structure refinement

Fully ionized scattering curves were used for the non-tetrahedrally coordinated cations, and both neutral and ionized scattering factors were used for the tetrahedrally coordinated cations and the oxygen atoms (Ungaretti 1980). *R* indices are of the standard form and are given as percentages.

All refinements were done in the space group *C*2/*m* according to the procedure of Hawthorne *et al.* (1993a). Final *R* indices and miscellaneous information are given in Table 2. Atomic positions and displacement factors are given in Table 3, refined site-scattering powers in Table 4, and selected interatomic distances and angles in Table 5.

THE T(3) SITE

Site population

The stereochemical details of the *T*(3) site are given in Table 5 and Figure 1. The *T*(3) site is surrounded by four anions, O(1A), O(1B) and 2 × O(3), in a tetrahedral arrangement with a <*T*(3)–O> distance of ~1.80 Å. The site-scattering power at *T*(3) varies considerably in the heated series of staurolite crystals, from zero to 19.2 epfu (electrons per formula unit), and yet the <*T*(3)–O> distance is fairly constant across the series. This finding suggests that the observed distance is not materially affected by the partial occupancy of the site (*i.e.*, by the presence of extensive vacancies, □), and that the species occupying *T*(3) has a mean bond-length of ~1.80 Å. Subtracting a mean radius of 1.36 Å for oxygen (radii from Shannon 1976) gives the mean radius of the *T*(2) cation as

TABLE 4. REFINED SITE-SCATTERING POWERS* IN HEATED STAUROLITE

Temp. (°C)	N**	25	500	600	700	800	900	950
M(1A)	4	52.48	52.97	53.33	53.78	54.02	54.07	53.57
M(1B)	4	53.33	53.30	53.52	53.86	54.05	54.05	53.54
M(2)	8	106.45	107.38	108.57	110.28	112.88	112.86	112.75
M(3A)	2	16.19	15.76	13.28	11.26	9.16	9.20	9.17
M(3B)	2	9.42	10.40	11.83	11.25	9.20	9.18	9.19
M(4A)	2	2.81	3.20	4.10	4.98	4.80	4.79	4.50
M(4B)	2	1.10	2.04	3.69	5.01	4.83	4.86	4.45
T(2)	4	88.08	85.54	77.21	66.03	59.49	58.47	61.23
T(3)	4	-	0.60	3.25	11.05	19.08	19.19	18.51
Total		329.86	331.19	326.78	327.50	327.51	326.67	326.91

* standard deviations are all ~0.02–0.08, depending on the equipoint rank of the site
** N is the number of sites in the structural formula (corresponding to the formula unit)

0.44 Å. This value is between those of $^{[4]}Fe^{3+}$ (r = 0.49 Å) and $^{[4]}Al$ (r = 0.39 Å), indicating that $T(3)$ is occupied by Al and Fe^{3+}.

Polyhedral linkage

The $T(3)O_4$ tetrahedron occurs within the "hydroxide" layer of the staurolite structure. It shares an edge with the $T(2)$ tetrahedron (Fig. 1) and shares faces with the adjacent $M(3A)$ and $M(3B)$ octahedra. In addition, it shares all four corners with $M(2)$ octahedra of the "kyanite" part of the structure.

Constraints on occupancy: cation–cation approaches

The close $T(3)$–$M(3A)$ and $T(3)$–$M(3B)$ approaches (Table 5) preclude simultaneous *local* occupancy of $T(3)$ and either $M(3A)$ or $M(3B)$. The short $T(3)$–$T(2)$ approach (Table 5) also indicates that simultaneous *local* occupancy of $T(3)$ and $T(2)$ is unfavorable.

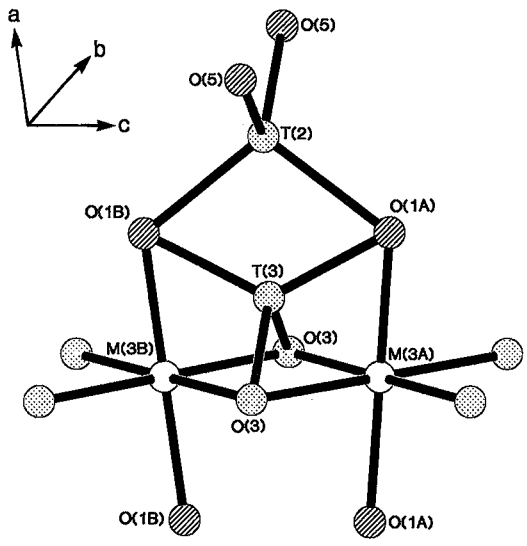

FIG. 1. The stereochemical details of the $T(3)$ site in the structure of oxidized staurolite; all neighboring cation sites are shown, but not all of these are locally occupied.

CHANGES IN SITE POPULATIONS ON OXIDATION

Inspection of Figures 2, 3 and 4 show that *all* cation sites, except $T(1)$, are significantly involved in the oxidation process, and that no further oxidation–dehydrogenation is observed beyond 900°C. Summing the A and B sites for simplicity, we see the following changes in site scattering (Table 4) between the unheated and the (900°C)-heated structures: $M(1) \approx 2$, $M(2) \approx 6$, $M(3) \approx -7$, $M(4) \approx 6$, $T(2) \approx -29$, $T(3) \approx 19$ epfu. Thus although the *principal* change must involve cation transfer from the $T(2)$ site to the $T(3)$ site, it is apparent that a complicated cation-exchange process occurs.

We can get an idea of the changes in the site populations upon heating by comparing the variation in the site-scattering powers with the corresponding changes in the mean bond-lengths. For these, we will consider each pair of A and B sites together, as Hawthorne *et al.* (1993a, b) have shown that the mean bond-lengths of the individual A and B polyhedra are affected by the degree of order of the overall structure, whereas the mean of each pair is independent of the degree of order.

M(1) site

Upon heating, the $M(1)$ site-scattering increases (Fig. 2), whereas the $\langle M(1)\text{–O}\rangle$ bond-length decreases (Fig. 4). This behavior indicates that a heavier (larger Z), smaller cation is replacing a larger, lighter (smaller Z) cation. $M(1)$ is occupied predominantly by Al, with small amounts of Mg. The incoming cation must be Fe^{3+} (presumably in the trivalent state, as oxidation–dehydrogenation is driving the changes), and therefore we have a $Fe^{3+} \rightleftharpoons Mg$ exchange at this site: the difference in the site-scatterings (2.31 epfu) is consistent with 0.16 Fe^{3+} being introduced and 0.16 Mg being removed. Note that this agrees with the initial site-populations (Table 6) proposed in Hawthorne *et al.* (1993a); the oxidation process thus involves complete removal of Mg from the $M(1)$ site(s).

M(2) site

There is a significant increase in the site scattering (Fig. 3), and the mean $\langle M(2)\text{–O}\rangle$ distance increases slightly (Fig. 4). The increase in scattering must be due to the introduction of Fe^{3+} replacing a lighter cation; therefore we have a $Fe^{3+} \rightleftharpoons Al$ exchange at this site involving $6.41/(Z^{Fe}–Z^{Al}) = 0.49$ apfu. A simple hard-sphere calculation suggests that this amount of exchange should increase the $\langle M(2)\text{–O}\rangle$ distance by ~0.007 Å, and that is exactly what is observed

TABLE 5. SELECTED INTERATOMIC DISTANCES (Å) IN HEATED STAUROLITE

Temp. (°C)	25	500	600	700	800	900	950
T(1)–O(2A)	1.632	1.634	1.632	1.632	1.631	1.631	1.631
T(1)–O(2B)	1.633	1.633	1.632	1.632	1.631	1.631	1.631
T(1)–O(3)	1.651	1.653	1.651	1.651	1.649	1.649	1.648
T(1)–O(4)	1.641	1.642	1.640	1.639	1.637	1.638	1.638
<T(1)–O>	1.639	1.640	1.639	1.638	1.637	1.637	1.637
M(1A)–O(2A) x2	1.938	1.939	1.940	1.936	1.931	1.931	1.930
M(1A)–O(4) x2	1.897	1.897	1.899	1.898	1.895	1.896	1.895
M(1A)–O(5) x2	1.894	1.894	1.894	1.895	1.894	1.896	1.894
<M(1A)–O>	1.910	1.910	1.911	1.909	1.906	1.908	1.906
M(1B)–O(2B) x2	1.947	1.947	1.943	1.936	1.930	1.931	1.930
M(1B)–O(4) x2	1.903	1.902	1.902	1.898	1.895	1.895	1.896
M(1B)–O(5) x2	1.897	1.898	1.894	1.895	1.893	1.896	1.894
<M(1B)–O>	1.916	1.916	1.911	1.909	1.906	1.907	1.906
M(2)–O(1A)	1.919	1.919	1.915	1.908	1.908	1.910	1.910
M(2)–O(1B)	1.918	1.918	1.916	1.908	1.908	1.911	1.911
M(2)–O(2A)	1.935	1.935	1.930	1.935	1.939	1.940	1.939
M(2)–O(2B)	1.921	1.923	1.927	1.936	1.939	1.939	1.941
M(2)–O(3)	1.875	1.873	1.875	1.880	1.883	1.882	1.882
M(2)–O(5)	1.868	1.868	1.871	1.884	1.894	1.893	1.894
<M(2)–O>	1.906	1.906	1.906	1.908	1.912	1.913	1.913
M(3A)–O(1A) x2	1.848	1.852	1.862	1.874	1.882	1.882	1.883
M(3A)–O(3) x4	2.027	2.032	2.042	2.053	2.062	2.062	2.063
<M(3A)–O>	1.968	1.972	1.982	1.994	2.002	2.002	2.003
M(3B)–O(1B) x2	1.867	1.866	1.865	1.873	1.882	1.883	1.883
M(3B)–O(3) x4	2.065	2.061	2.051	2.053	2.061	2.064	2.063
<M(3B)–O>	1.999	1.996	1.989	1.993	2.001	2.003	2.003
M(4A)–O(1A) x2	2.106	2.103	2.091	2.076	2.062	2.062	2.061
M(4A)–O(5) x4	2.196	2.194	2.188	2.168	2.154	2.154	2.156
<M(4A)–O>	2.166	2.163	2.155	2.138	2.124	2.123	2.125
M(4B)–O(1B) x2	2.084	2.085	2.087	2.077	2.063	2.061	2.061
M(4B)–O(5) x4	2.200	2.198	2.189	2.169	2.154	2.153	2.157
<M(4B)–O>	2.161	2.160	2.155	2.138	2.124	2.123	2.125
T(2)–O(1A)	2.035	2.030	2.013	1.956	1.920	1.921	1.921
T(2)–O(1B)	2.033	2.029	2.011	1.956	1.921	1.920	1.920
T(2)–O(5) x2	1.978	1.978	1.979	1.987	1.982	1.980	1.984
<T(2)–O>	2.006	2.003	1.995	1.971	1.951	1.950	1.952
T(3)–O(1A)	–	1.749	1.817	1.814	1.797	1.799	1.800
T(3)–O(1B)	–	1.811	1.811	1.815	1.798	1.797	1.798
T(3)–O(3) x2	–	1.834	1.785	1.780	1.792	1.793	1.793
<T(3)–O>	–	1.807	1.799	1.797	1.795	1.796	1.796
T(3)–M(3A)	–	1.755	1.737	1.716	1.716	1.716	1.716
T(3)–M(3B)	–	1.823	1.736	1.717	1.715	1.715	1.715
T(3)–T(2)	–	1.984	2.053	2.025	1.997	1.999	1.998

(Table 5, Fig. 4). Later, we will see that the overall exchange of cations accompanying oxidation–dehydrogenation involves the increase in proportion of cations at the $M(4)$ sites, both of which preferentially accept divalent cations. Hence it is likely that the Mg at $M(2)$ is replaced by Al, as is the case for $M(1)$. Replacement of the small amount of Mg initially at $M(2)$ by Al will not have a significant effect on $<M(2)–O>$ [<0.001 Å], and hence we cannot be certain of this particular exchange; however, as

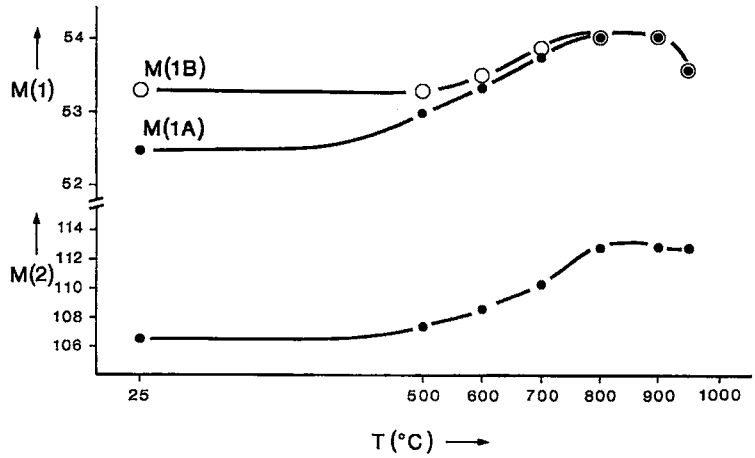

FIG. 2. The variation in the cation site-scattering as a function of temperature of heating in the "kyanite" layer of the staurolite structure.

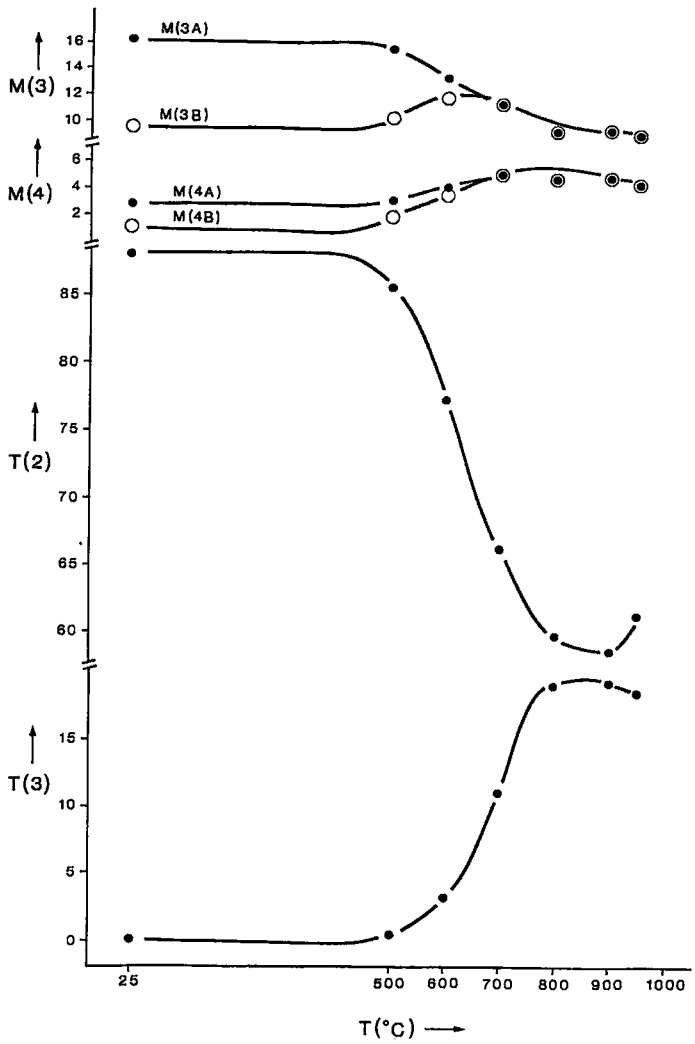

FIG. 3. The variation in the cation site-scattering as a function of temperature of heating in the "hydroxide" layer of the staurolite structure.

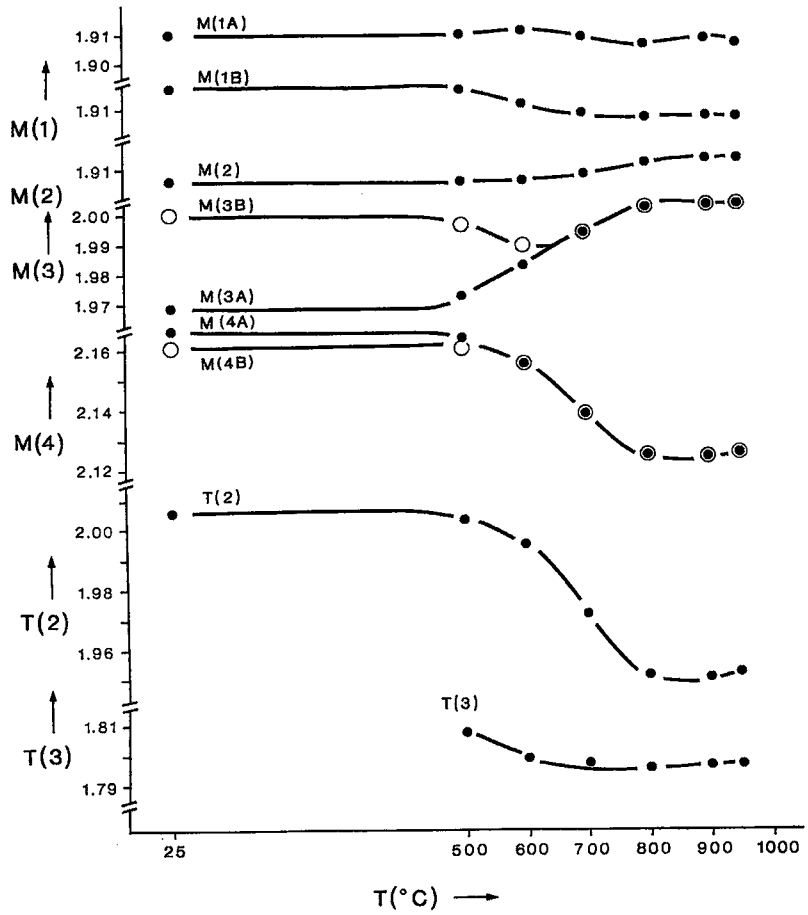

FIG. 4. The variation in mean bond-lengths as a function of temperature of heating at selected cation-sites in staurolite.

TABLE 6. SITE POPULATIONS (APFU) IN STAUROLITE FOR THE 25°C AND 900°C STRUCTURE REFINEMENTS

T (°C)		25	900			25	900
M(1)	Al	7.78	7.78	T(1)	Si	7.58	7.58
	Mg	0.16	–		Al	0.42	0.42
	Fe*	0.06	0.22				
				T(2)	Fe*	2.76	1.62
M(2)	Al	7.77	7.32		Zn	0.04	0.04
	Mg	0.04	0.00		Mg	0.38	0.30
	Fe*	0.19	0.68		Al	0.52	0.71
					□	0.30	1.33
M(3)	Al	1.64	1.08				
	Mg	0.08	0.08	T(3)	Fe^{3+}	–	0.35
	Fe*	0.12	0.12		Al	–	0.79
	□	0.16	0.72		□	4.00	2.86
M(4)	Fe^{2+}	0.15	0.25				
	Mg	–	0.28				
	□	3.85	3.47				

Fe* = Fe^{3+} + Ti^{4+} + Cr; Fe* = Fe^{2+} + Fe^{3+} + Co

noted above, it is in line with the exchange observed at *M*(1).

M(3) site

The significant loss of scattering at *M*(3) upon heating (Fig. 3) must involve replacement of $7.23/Z^{Al}$ = 0.56 apfu of Al by □ (vacancies). This produces a significant change in the <*M*(3)–O> bond-length (Fig. 4). Hawthorne *et al.* (1993b) have calculated the "radius" of a □ at the *M*(3) site; a value of 0.67 Å was obtained. Using this value, the loss of 0.56 Al pfu from the *M*(3) site should result in an increase in <*M*(3)–O> of ~0.019 Å, which agrees with the observed change of 0.020 Å (Table 5).

T(2) site

There is a large reduction in the $T(2)$ scattering and in the <$T(2)$–O> bond length (Tables 4, 5, Figs. 2, 4). Assuming that the loss of scattering power is completely associated with oxidation of $^{T(2)}Fe^{2+}$ by dehydrogenation involving O(1*A*) and O(1*B*), and subsequent migration of Fe^{3+} elsewhere, the $T(2)$ site loses $29/Z^{Fe} = 1.14$ Fe^{2+} apfu.

M(4) site

The refined site-scattering values (Table 4, Fig. 3) indicate that the $M(4)$ site population increases upon heating, but the site scattering and mean bond-lengths (Fig. 4) do not give sufficient information to calculate the site populations. However, the bond-valence model (discussed later) introduces certain stoichiometric relationships between the site populations of $M(3)$, $M(4)$ and $T(3)$, and these provide sufficient constraints to assign consistent site-populations.

T(3) site

The $T(3)$ site is vacant in the unheated structure, but shows a large increase in scattering with heating above ~500°C. As with $M(4)$, site populations may be assigned from the refined site-scattering and the stoichiometric constraints of the bond-valence model.

Complete site-populations are given in Table 6 for both the unheated and the heated (900°C) structures.

The Oxidation–Dehydrogenation Mechanism

The $T(2)$ atom bonds to O(1*A*) and O(1*B*) (Fig. 1), one of which is usually a hydroxyl anion. The combined oxidation–dehydrogenation proceeds *via* the process

$$^{T(2)}Fe^{2+} + {}^{O(1)}OH^- \rightarrow {}^{T(2)}Fe^{3+} + {}^{O(1)}O^{2-} + H\uparrow \quad (1)$$

in which an electron transfers from Fe^{2+} to the anion, releasing hydrogen to migrate through the structure to the surface of the crystal. This results in a very large reduction in cation size at the $T(2)$ site. The $T(2)$ tetrahedron is relatively large, with significant positional disorder of the constituent cations within the polyhedron (Smith 1968); Hawthorne *et al.* (1993c) have rationalized this disorder on the basis of patterns of local order within the "hydroxide" part of the structure. We examine the oxidation–dehydrogenation process and its accompanying rearrangement of cations in the same way.

A bond-valence model

Hawthorne *et al.* (1993c) have shown that the two most common patterns of order in the "hydroxide" layer of staurolite involve local occupancy of $T(2)$, $M(3A)$ and H(1*B*) [and the corresponding $T(2)$–$M(3B)$–H(1*A*) arrangement]. The bond-valence table for this arrangement is shown as Table 7, using a simple Pauling model. What happens when Fe^{2+} at $T(2)$ is oxidized to Fe^{3+} and the locally associated hydrogen atom is lost *via* the concomitant dehydrogenation? The corresponding bond-valence arrangement is shown in Table 8a, omitting the O(2*A*), O(2*B*) and O(4) anions that do not coordinate cation sites involved in the major changes accompanying heating. There are significant bond-valence excesses at O(1*A*) and O(5), and a bond-valence deficiency at O(1*B*). In addition, the O(3) anion is effectively underbonded because the 0.5 v.u. contribution from $M(3A)$ (Table 8a) is significantly decreased by the long $M(3A)$–O(3) distance. The geometry and connectivity of the structure do not allow the structure to relax and reduce the bond-valence deviations from ideality (Table 8a), and hence a rearrangement of cations is

TABLE 7. BOND-STRENGTH TABLE FOR UNHEATED STAUROLITE SHOWING THE MOST COMMON LOCAL ARRANGEMENT*

	M(1A)	M(1B)	M(2)	Si	Σ**	M(3A)	T(2)	H(1B)	Σ
O(1A)			1/2×2→		1.0	1/2×2↓	1/2		2.00
O(1B)			1/2×2→		1.0		1/2	0.8	2.30
O(2A)	1/2×2↓		1/2	1	2.0				2.00
O(2B)		1/2×2↓	1/2	1	2.0				2.00
O(3)			1/2	1	1.5	1/2×2↓		0.2	2.20
O(4)	1/2×2↓	1/2×2↓		1	2.0				2.00
O(5)	1/2×2↓	1/2×2↓	1/2		1.5		1/2×2↓		2.00

* there is an analogous arrangement with M(3B) and H(1A) both occupied; unoccupied cation sites are not shown

** sum of the bond strengths for the kyanite part of the staurolite structure

TABLE 8. POSSIBLE BOND-STRENGTH ARRANGEMENTS IN THE "HYDROXIDE" LAYER OF HEATED (OXIDIZED) STAUROLITE*

	Σ**	M(3A)	T(2)	H(1B)	T(3)	M(4A)	Σ
Arrangement (a): T(2) cation oxidized, H(1B) vacant							
O(1A)	1.00	$1/2^{\times 2}\downarrow$	3/4				2.25
O(1B)	1.00		3/4	–			1.75
O(3)	1.50	$1/2^{\times 1}\downarrow$		–			2.00
O(5)	1.50		$3/4^{\times 2}\downarrow$				2.25
Arrangement (b): M(3A) vacant, T(3) occupied							
O(1A)	1.00	–	–		3/4		1.75
O(1B)	1.00		–	–	3/4		1.75
O(3)	1.50	–		–	$3/4^{\times 2}\downarrow$		2.25
O(5)	1.50		–				1.50
Arrangement (c): T(3) occupied, M(4A) occupied							
O(1A)	1.00	–	–		3/4	$1/2^{\times 2}\downarrow$	2.25
O(1B)	1.00		–	–	3/4		1.75
O(3)	1.50	–		–	$3/4^{\times 2}\downarrow$		2.25
O(5)	1.50		–			$1/2^{\times 1}\downarrow$	2.00

* there is an analogous arrangement with M(4B) occupied
** bond-strength sum from the kyanite part of the structure

necessary. Table 8b shows the situation with the *T*(3) occupied and the *M*(3*A*) site vacant [as required from the very short *T*(3)–*M*(3*A*) approach]. With this arrangement, the bond-valence deviations are larger than before; in particular, the O(5) anion, a very sensitive anion in terms of structural arrangements, is greatly underbonded at 1.50 v.u. However, the arrangement in Table 8b has displaced a cation from *M*(3*A*), and this may compensate for the loss of bond-valence to the O(5) anion. This may be done by occupancy of the *M*(4*A*) site by a divalent cation that is displaced from another site [*e.g.*, *M*(1) or *M*(2)] by the Al evicted from *M*(3*A*). This situation is shown in Table 8c; the bond-valence sum around O(5) is now at the ideal value of 2.0 v.u. The bond-valence sum around O(3) is now 2.25 v.u., but the *T*(1)–O(3) bond is the longest of the *T*(1)–O bond lengths in the staurolite structure (Table 5); hence the structure inherently contains the structural relaxation necessary for O(3) to achieve an ideal incident bond-valence. Thus although the arrangements in Tables 8a and 8c show identical deviations from ideality for a formal Pauling bond-strength model, only the arrangement in Table 8c can approach an ideal bond-valence distribution *via* structural relaxation.

The exchange of Mg for Fe^{3+} at the *M*(1) sites can also be explained using this mechanism. Both the *M*(1*A*) and *M*(1*B*) cations bond to O(5), which loses incident bond-valence when *T*(2) becomes vacant. Replacement of Mg by Fe^{3+} will relieve the *local* bond-valence deficiency caused by Mg at the *M*(1) sites. The exchange of Fe^{3+} for Al at *M*(2) cannot be explained on this basis, and presumably results from steric accommodation.

Implications for site populations

The model proposed in Table 8 requires that the site population of *T*(3) is twice that of *M*(4), and that the vacancy introduced at *M*(3) is half the site population of *T*(3). The changes in the site scattering upon heating (Table 4) at *M*(3) and *T*(2), together with the observed scattering at *M*(4), are of the correct order for this model: *M*(3) = –7.23 epfu (= 0.56 Al), *M*(4) = 9.65 epfu, *T*(3) = +19.19 epfu. Assuming exact adherence to the model thus allows us to assign specific site-populations to *M*(4) and *T*(2); the values are given in Table 6. According to our model, the value of the total *M*(4) population (0.57 apfu) should be equal to the vacancy content of the *M*(3) site induced by heating; this value is 0.56 □ pfu (Table 6), supporting the validity of the model and the assigned site-populations.

Structural Effects of Heating

Staurolite can be considered as an order–disorder series, with fully ordered monoclinic (*C2/m*) staurolite and fully disordered orthorhombic (*Cccm*) staurolite as ideal end-members (Hawthorne *et al.* 1993b). The primary order-parameter of the (putative) phase-transition involves Al–□ ordering over the *M*(3*A*) and *M*(3*B*) sites. Thus on heating a crystal of staurolite, there is the potential to change the degree of Al–□ order over *M*(3*A*) and *M*(3*B*) [together with other coupled ordering-processes within the crystal]. In addition, staurolite also oxidizes *via* the coupled oxidation–dehydrogenation mechanism discussed above. Consequently, the response of the structure to heating involves a combination of these two processes. For convenience of expression, we may distinguish between ordering associated with each process with the terms *convergent* ordering and *nonconvergent* ordering.

Convergent ordering

The cation sites involved in the order–disorder transition in the staurolite series are the *M*(3*A*)–*M*(3*B*), *M*(4*A*)–*M*(4*B*) and *M*(1*A*)–*M*(1*B*) pairs. For *M*(3), there is only a slight change in site scattering below 500°C. Between 500 and 600°C, the site-scattering values converge strongly, initially in a symmetrical way (Fig. 3); however, at ~575°C, the scattering at *M*(3*B*) begins to deviate from this symmetrical relationship, increasing less strongly and reaching a maximum at ~600°C, and then decreasing again until it becomes identical with the *M*(3*A*) scattering at (or slightly below) 700°C. Extrapolating the initial symmetrical convergence of the *M*(3*A*) and *M*(3*B*) site-scattering values gives a point of intersection at ~625°C, suggesting that this is the temperature

at which the structure would become orthorhombic in the absence of oxidation–dehydrogenation. Extrapolation of the <*M*(3*A*)–O> and <*M*(3*B*)–O> values and of the initial trend of the β angle also supports a transition temperature of ~625°C.

The behavior of *M*(4*A*) and *M*(4*B*) is rather different (Fig. 3). They show no sign of symmetrical convergence, but site-scattering values begin to increase somewhat below 500°C, eventually merging at (or slightly below) 700°C.

Nonconvergent ordering

The behavior of the site-populations at *M*(3) as a function the temperature of heating indicates that convergent ordering initially proceeds with heating, but is strongly perturbed at ~575°C, presumably by cation exchange involving the oxidation–dehydrogenation process. This perturbation will involve the migration of Fe^{3+} from *T*(2) to *T*(3), with the resultant removal of Al from *M*(3) [and, to a lesser extent, *M*(2)].

However, the variation in the site scattering at *T*(2) shows that oxidation–dehydrogenation starts below 500°C, and thus must proceed without strongly perturbing the Al–□ disordering at *M*(3) for ~100°C. The initial site-populations for *M*(3*A*) and *M*(3*B*) show 0.16 vacancies present in excess of 2 □ pfu. Thus in local arrangements involving these vacancies at *M*(3), *T*(3) could be occupied *without* the need for displacing an Al atom from the adjacent *M*(3*A*) or *M*(3*B*) site. Thus the increase in site scattering of *M*(4*A*), *M*(4*B*) and *T*(2) below ~575°C, which progresses without perturbing the Al–□ disordering over *M*(3*A*) and *M*(3*B*), must involve locally associated pairs of vacancies at *M*(3*A*) and *M*(3*B*). This behavior suggests that oxidation–dehydrogenation initially takes place at

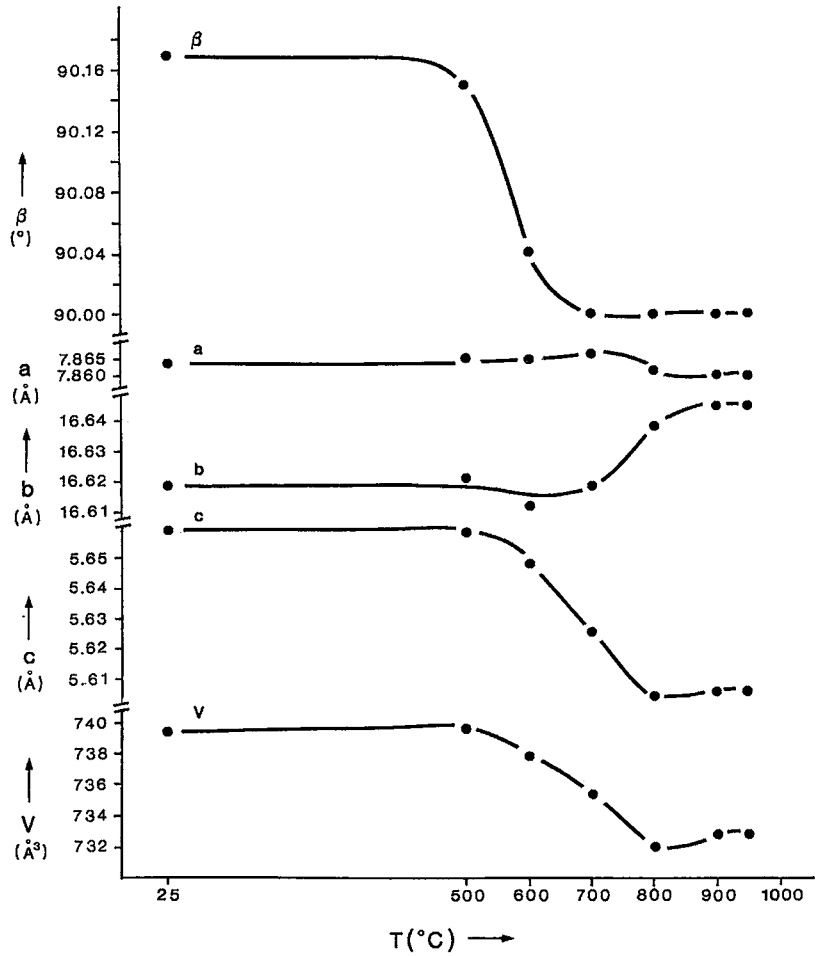

FIG. 5. The variation in cell dimensions of staurolite as a function of temperature of heating.

these local arrangements before becoming more extensive at higher temperatures.

Effect on unit-cell dimensions

The behavior of cell dimensions on heating is very similar to that found by Gibbons *et al.* (1981). There is a significant reduction in the unit-cell volume upon heating (Fig. 5), reflecting the decrease in size of Fe upon oxidation and the concomitant loss of hydrogen on dehydrogenation. In addition, the gradually increasing disorder within the structure promotes an approach to orthorhombic symmetry that is reflected in the decrease of the β angle, a measure of the spontaneous strain, which attains 90° at ~700°C. The principal change involves *c*, which contracts by ~1%. This change can be understood by inspecting a view of the "hydroxide" layer down [010] (Fig. 6). A large (Fe^{2+}) cation is removed from the *T*(2) site and small cations occupy the *T*(3) and *M*(4) sites. Thus the long O–O separation involving the edge of the *T*(2) tetrahedron can relax to form an edge of the much smaller *T*(3) tetrahedron, and the whole "hydroxide" layer can contract in the *c* direction. The initial contraction of *c* is small, when the cation rearrangements involve paired vacancies at *M*(3); however, when the rearrangements begin to involve significant decrease in the *M*(3) site-populations, then *c* decreases more rapidly. The smaller responses of *a* and *b* seem to be the result of the structure simultaneously accommodating the more important changes in *c* and *V*.

Summary

Crystal-structure refinement of staurolite annealed in air at a series of increasing temperatures shows the following changes to occur:

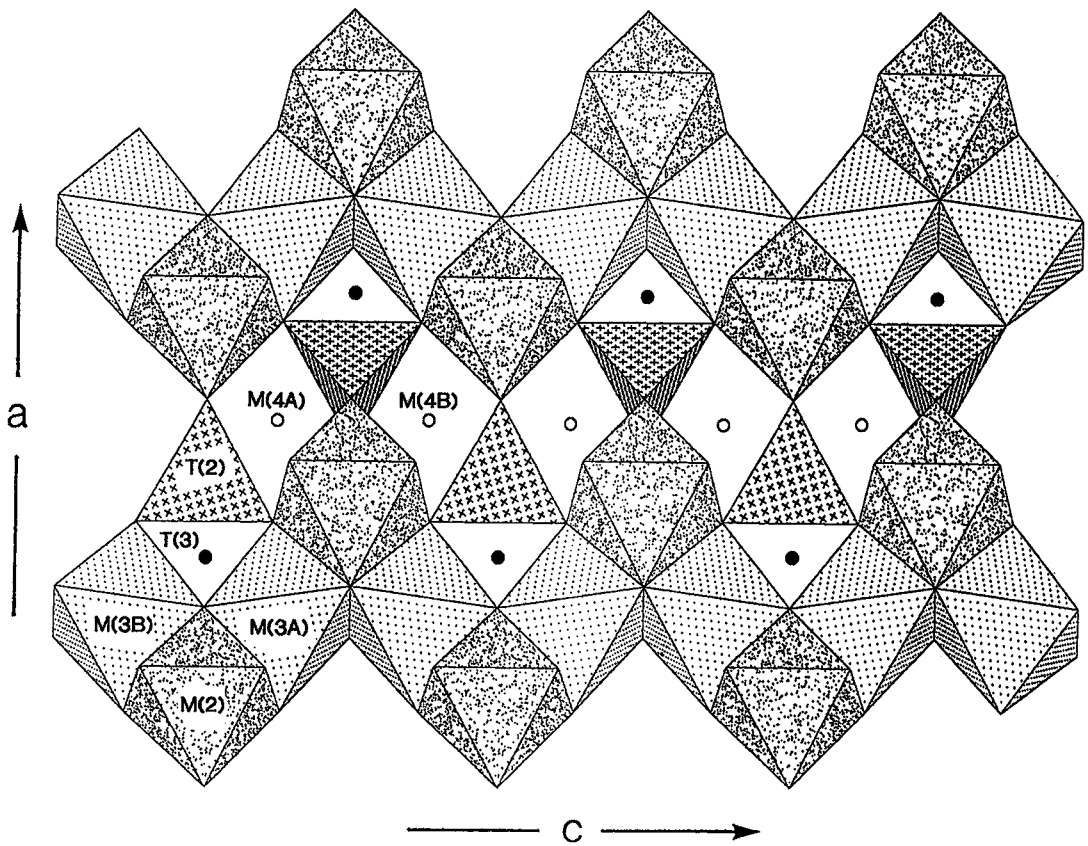

FIG. 6. The "hydroxide" layer in the staurolite structure, viewed down [010]; *M*(3) octahedra are lattice-dot shaded, *T*(2) tetrahedra are cross-shaded, *M*(2) octahedra are random-dot shaded, *T*(3) sites are shown as solid circles, and *M*(4) sites are shown as hollow circles.

(1) Below 575°C, there is convergent ordering at the $M(3A)$–$M(3B)$ and $M(4A)$–$M(4B)$ pairs of sites; extrapolation to higher temperatures suggests complete convergence at ~625°C.
(2) Cation rearrangements associated with oxidation–dehydrogenation begin to obscure convergent ordering at 500–575°C.
(3) Staurolite oxidizes *via* a dehydrogenation process of the form $Fe^{2+} + OH^- \rightarrow Fe^{3+} + O^{2-} + H\uparrow$.
(4) There is a newly occupied site, $T(3)$, in the annealed structure, and the occupancy of this site increases with increasing temperature of annealing.
(5) The $T(3)$ cation is tetrahedrally coordinated by oxygen anions, with a $<T(3)–O>$ distance of ~1.80 Å; the resulting tetrahedron shares faces with the $M(3A)$ and $M(3B)$ octahedra, and an edge with the $T(2)$ tetrahedron.
(6) The $<T(3)–O>$ distance indicates occupancy of $T(3)$ by Al and Fe^{3+}.
(7) The site populations at the $M(1A)$, $M(1B)$, $M(2)$, $M(3A)$, $M(3B)$, $M(4A)$, $M(4B)$, $T(2)$ and $T(3)$ sites all change significantly on heating.
(8) Upon oxidation–dehydrogenation, Fe^{3+} is lost from $T(2)$, and Al is lost from $M(3A)$, $M(3B)$ and $M(2)$, whereas increased amounts of Fe^{3+} and Al occur at $T(3)$, $M(4A)$ and $M(4B)$; this exchange results in reasonable satisfaction of local bond-valence requirements.
(9) The presence of atoms at the $T(3)$ site in natural staurolite may be an indicator of postcrystallization oxidation–dehydrogenation.

Acknowledgements

We thank the reviewers, Mikes Henderson and Holdaway, for suggestions that significantly improved the clarity of this manuscript. Financial support for FCH was provided by a Killam Fellowship, a CNR–NATO Fellowship, and the Natural Sciences and Engineering Research Council of Canada.

References

Alexander, V.D. (1989): Iron distribution in staurolite at room and low temperatures. *Am. Mineral.* **74**, 610-619.

Dutrow, B.L., Holdaway, M.J. & Hinton, R.W. (1986): Lithium in staurolite and its petrologic significance. *Contrib. Mineral. Petrol.* **94**, 496-506.

Dyar, M.D., Perry, C.L., Rebbert, C.R., Dutrow, B.L., Holdaway, M.J. & Lang, H.M. (1991): Mössbauer spectroscopy of synthetic and naturally occurring staurolite. *Am. Mineral.* **76**, 27-41.

Gibbons, K., Dempsey, M.J. & Henderson, C.M.B. (1981): The thermal expansion of staurolite, $Fe_4Al_{18}Si_8O_{44}(OH)_4$. *Mineral. Mag.* **44**, 69-72.

Hawthorne, F.C., Ungaretti, L., Oberti, R., Caucia, F. & Callegari, A. (1993a): The crystal chemistry of staurolite. I. Crystal structure and site populations. *Can. Mineral.* **31**, 551-582.

———, ———, ———, ——— & ——— (1993b): The crystal chemistry of staurolite. II. Order – disorder and the orthorhombic → monoclinic phase transition. *Can. Mineral.* **31**, 583-595.

———, ———, ———, ——— & ——— (1993c): The crystal chemistry of staurolite. III. Local order and chemical composition. *Can. Mineral.* **31**, 597-616.

Henderson, C.M.B., Charnock, J.M., Smith, J.V. & Greaves, G.N. (1993): X-ray absorption spectroscopy of Fe, Mn, Zn, and Ti structural environments in staurolite. *Am. Mineral.* **78**, 477-485.

Holdaway, M.J., Dutrow, B.L., Borthwick, J., Shore, P., Harmon, R.S. & Hinton, R.W. (1986a): H content of staurolite as determined by H extraction line and ion microprobe. *Am. Mineral.* **71**, 1135-1141.

———, ——— & Hinton, R.W. (1988): Devonian and Carboniferous metamorphism in west-central Maine: the muscovite–almandine geobarometer and the staurolite problem revisited. *Am. Mineral.* **73**, 20-47.

———, ——— & Shore, P. (1986b): A model for the crystal chemistry of staurolite. *Am. Mineral.* **71**, 1142-1159.

Pigage, L.C. & Greenwood, H.J. (1982): Internally consistent estimates of pressure and temperature: the staurolite problem. *Am. J. Sci.* **282**, 943-969.

Shannon, R.D. (1976): Revised effective ionic radii and systematic studies of interatomic distances in halides and chalcogenides. *Acta Crystallogr.* **A32**, 751-767.

Smith, J.V. (1968): The crystal structure of staurolite. *Am. Mineral.* **53**, 1139-1155.

Ståhl, K., Kvick, Å. & Smith, J.V. (1988): A neutron diffraction study of hydrogen positions at 13 K, domain model, and chemical composition of staurolite. *J. Sol. State Chem.* **73**, 362-380.

Ungaretti, L. (1980): Recent developments in X-ray single-crystal diffractometry applied to the crystal-chemical study of amphiboles. *God. Jugoslav. Kristalogr.* **15**, 29-65.

Received March 22, 1993, revised manuscript accepted October 15, 1993.